УДК 621.926.2
DOI: https://doi.org/10.32347/tb.2025-43.0604

[1]Ivan Nazarenko,
Doctor of Technical Sciences, Professor of the Department of Machines and Equipment for Technological Processes, https://orcid.org/0000-0002-1888-3687, e-mail: nazarenko.ii@knuba.edu.ua

[1]Yevhen Mishchuk,
Candidate of Technical Sciences, Associate Professor of the Department of Machines and Equipment for Technological Processes, https://orcid.org/0000-0002-7850-0975, e-mail: mischuk.ieo@knuba.edu.ua

[1]Petro Ladkin,
Postgraduate student, the Department of Machines and Equipment for Technological Processes, https://orcid.org/0009-0006-1448-3957, e-mail: ladkin_py-2022@knuba.edu.ua

[1]Kyiv National University of Construction and Architecture, Povitryanih Sil ave., 31, Kyiv, 03037, Ukraine

MODELING THE FAILURE PROCESS OF MATERIALS WITH DIFFERENT PHYSICAL AND MECHANICAL PROPERTIES UNDER STATIC LOADING CONDITIONS

ABSTRACT. *The main technical indicator of a crushing machine is the specific energy consumption per unit of the product obtained. In connection with the development of technologies and the increase in construction volumes, engineers are faced with the task of optimizing the designs of crushing machines in order to reduce energy consumption for the process of material destruction. That is, the study of the use of various rheological models of the material in the process of crushing and taking into account the geometry of the surface of the working bodies of crushing machines is an urgent task today. The paper considers the stress and deformation patterns of various rheological models used to describe rocks under static loading conditions. The parameters of the Coulomb-Mohr rheological model and the influence of the cohesive strength and the angle of internal friction on the destruction process are analyzed. Graphs of the dependence of residual cohesion on the plastic deformation of the material are constructed under the condition of different values of the effective plastic deformation. The loading of the material by the wedge and flat profiles of the crushing plates is estimated. The dependence is given that determines the rational width of the contact surface of the crushing plates depending on the loading and the physical and mechanical properties of the contacting bodies.*

Keywords: *rheological model, finite element method, cohesion, angle of internal friction, plastic deformation, stress.*

МОДЕЛЮВАННЯ ПРОЦЕСУ РУЙНУВАННЯ МАТЕРІАЛІВ ІЗ РІЗНИМИ ФІЗИКО-МЕХАНІЧНИМИ ВЛАСТИВОСТЯМИ В УМОВАХ СТАТИЧНОГО НАВАНТАЖЕННЯ

АНОТАЦІЯ. *Основним технічним показником дробильної машини є питома витрата енергії на одиницю отриманого продукту. У зв'язку з розвитком технологій та збільшенням обсягів будівництва, перед інженерами постає завдання оптимізації конструкцій дробильних машин з метою зменшення енерговитрат на процес руйнування матеріалу. Тобто, дослідження використання різних реологічних моделей матеріалу в процесі дроблення та врахування геометрії поверхні робочих органів дробарок є актуальним завданням сьогодення. У роботі розглянуто картини напружень та деформацій різних реологічних моделей, що використовуються для опису гірських порід в умовах статичного навантаження. Проаналізовано параметри реологічної моделі Кулона-Мора та вплив когезійної міцності та кута внутрішнього тертя на процес руйнування. Побудовано графіки залежності залишкової когезії від пластичної деформації матеріалу за умови різних значень ефективної пластичної деформації. Оцінено навантаження матеріалу клиновими та плоскими профілями дробильних плит. Наведено залежність, яка визначає раціональну ширину контактної поверхні дробильних плит залежно від навантаження та фізико-механічних властивостей контактуючих тіл.*

Ключові слова: *реологічна модель, метод скінченних елементів, когезія, кут внутрішнього тертя, пластична деформація, напруження.*

1. Problem statement. The main technical indicator of a crushing machine is the specific energy consumption per unit of the product obtained. In connection with the development of technologies and the increase in construction volumes, engineers are faced with an urgent task, which is to optimize the designs of crushing machines in order to reduce energy consumption for the process of material destruction. The study of the process of energy consumption for crushing is a rather complex task, since energy consumption depends on a number of factors (heterogeneity of a piece of material, the presence of cracks, the geometry of the surface of the piece and the crushing elements of the machine, etc.), which change during the operation of the crusher. For example, a greater amount of energy is spent on the destruction of large pieces of material than on the destruction of smaller pieces, which is associated with the presence of a significant number of cracks in large pieces. The crushing process can be described as follows. First, external forces applied to a piece of material deform and break the protruding edges of a piece of material of irregular shape. Then, after the external forces reach the strength limit of the material, it is destroyed into small pieces. To determine the energy required for grinding, four basic laws of destruction are used, depending on the conditions of the working process. In addition, there are a significant number of variations of the basic laws. However, each of the laws covers only part of the complex processes that occur during the grinding of materials and does not reflect the overall picture of destruction. Therefore, the current task today is to study the use of various rheological models of the material in the grinding process and taking into account the geometry of the surface of the working bodies of crushing machines.

2. Review of Recent Studies and Publications. In the work [1], a review of the energy laws of material destruction in accordance with different types of crushing machines is made. The disadvantage of the work is the lack of analysis of rheological models and description of the interaction of the working bodies of crushing machines with the material. In the source [2], studies of the destruction between material particles in the crushing chamber of a cone crusher are presented. The authors prove the hypothesis that the destruction of the material under compressed conditions changes the nature of the stress state, the granulometric composition of the crushing product and affects energy consumption. The disadvantage of the study is the lack of consideration of the destruction of various materials based on their rheological models and taking into account the conditions of the process and the crushing chamber of the cone crusher. In the following work [3], a model of material destruction in the crushing chamber of an impact crusher is considered. The crusher operating process is taken into account by introducing a classification function that depends on the average impact energy per unit mass, the rotor speed and the material feed rate. The disadvantages of the model are that it does not take into account the interaction of material particles with each other and the geometry of the particles. The source [4] provides a review of scientific works that consider various methods and approaches used to study the mechanism of soil failure. The review covers two areas of modeling: 1) DEM modeling of brittle soil; 2) failure of continuum models. The disadvantages include the fact that the review of failure models was performed only for soils. A numerical study of the mechanism of particle failure under load is considered in [5]. The study is more aimed at identifying the mechanisms of crack formation in the particle. Due to the use of RFPA2D, the heterogeneity of the particle is taken into account during failure. The disadvantages are that the interaction between particles, the geometry of the crushing chamber and the parameters of the crusher are not taken into account, and the problem is solved in a two-dimensional formulation. Numerical modeling of material failure using the DEM method in the crushing chamber of a jaw and cone crusher is considered in [6]. The disadvantages of the work include the use of a proprietary software product to perform DEM simulation, although on the other hand the authors state that their research code can model a significant number of particles. Another disadvantage is the lack of research on the continuum model of the material, which may be associated with the entry of a solid particle of material into the crushing chamber. In [7], studies on the destruction of rocks by various methods (compression and impact) are presented. The degree of material damage, the dependence of damage on the type of load and the impact on the final product are assessed. The disadvantages include not taking into account many processes that occur in the crushing chamber, the

destruction of particles due to interaction with each other and the rheological properties of rocks. In [8], the destruction of materials in the crushing chamber of an impact crusher is considered, in order to determine energy costs. It was established that the destruction of materials by impact with friction minimization reduces energy costs. The disadvantages include considering the destruction problem only for the impact crusher, not taking into account the geometry of the crushing chamber and the material particle.

3. Purpose of work. To determine the regularities of the destruction process of materials with different physical and mechanical properties and under conditions of different geometry of crushing plates.

4. Materials and methods. The main materials for the analysis are scientific, technical and reference literature on domestic and foreign samples of modern crushing equipment. The main methods used in the work are the use of mathematical analysis in calculating the parameters of the mechanical mode of crushing machines. To perform calculations and plot graphs, software was used Ansys 2021, Wolfram Mathematica 11 and Excel 2016.

5. Results.

Let us consider modeling of working environments using various rheological models [8]. We will take granite as the material model, and a beam on two supports with a load applied to the center as the loading scheme. The modeling process itself will be performed in the Ansys R2021 software environment.

Let us start by considering the classical model – the Hooke model. For this purpose, Ansys has a ready-made rheological model – Isotropic Elasticity. The physical properties for granite will be the following – density (ρ =2600 km/m3), elastic modulus – 50000 MPa, Poisson's ratio – 0.27. Fig. 1, a shows the picture of stresses and deformations that occur in the experimental sample (granite). To reproduce the picture of possible stresses and deformations, a force within 30 kN was applied. The material for the wedge and supporting elements is taken as carbon steel. The stress pattern corresponds to their classical distribution under the action of a concentrated force on the elastic space.

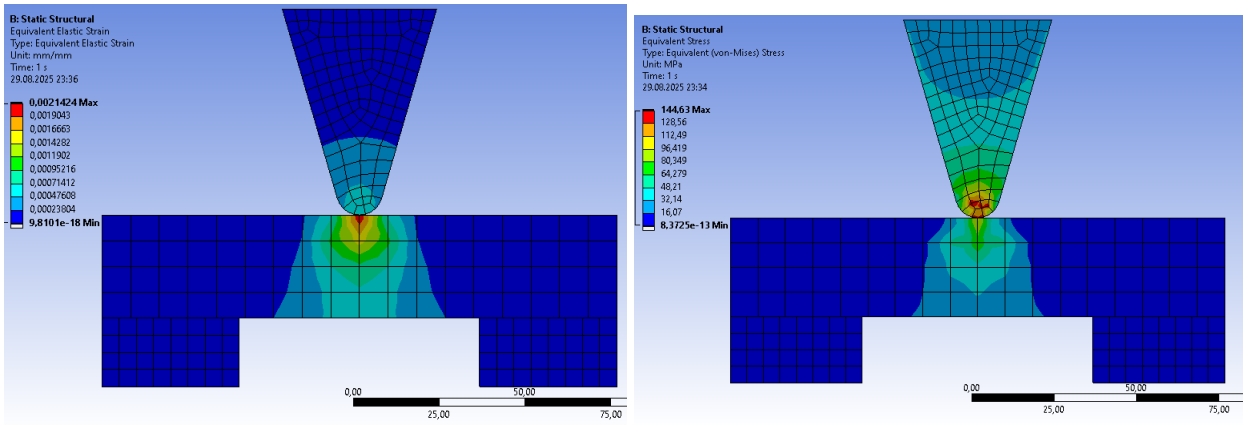

a b

Fig. 1. FEM model of a granite sample using Hooke's rheological model:
a – deformation field; b – stress field.

The graph of the dependence of stresses on deformations is presented in Fig. 2. The graph shows a directly proportional dependence of stress on deformation.

There are no rheological models of Saint-Venant or Prandtl in the Ansys library. The solution in this case is to use the models - Bilinear Isotropic Hardening or Multilinear Isotropic Hardening. These two models reproduce the plastic behavior of the material and, under appropriate boundary conditions, completely repeat the Prandtl or Saint-Venant model.

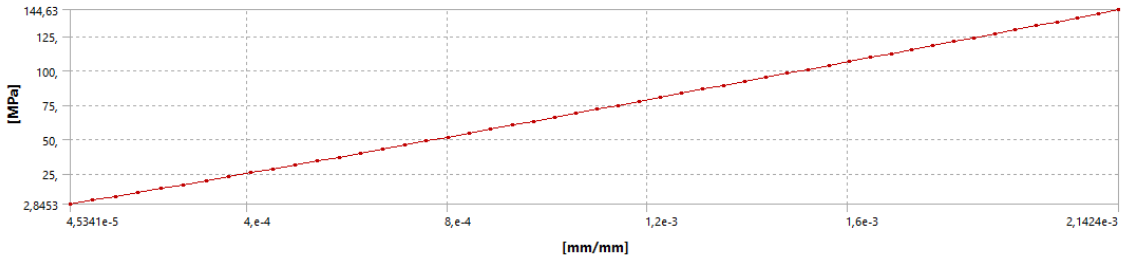

Fig. 2. Graph of the dependence of the change in stress on strain for the Hooke rheological model

To reproduce the Prandtl model, a simpler option is to use Bilinear Isotropic Hardening. The elastic and plastic deformations are shown in Fig. 3.

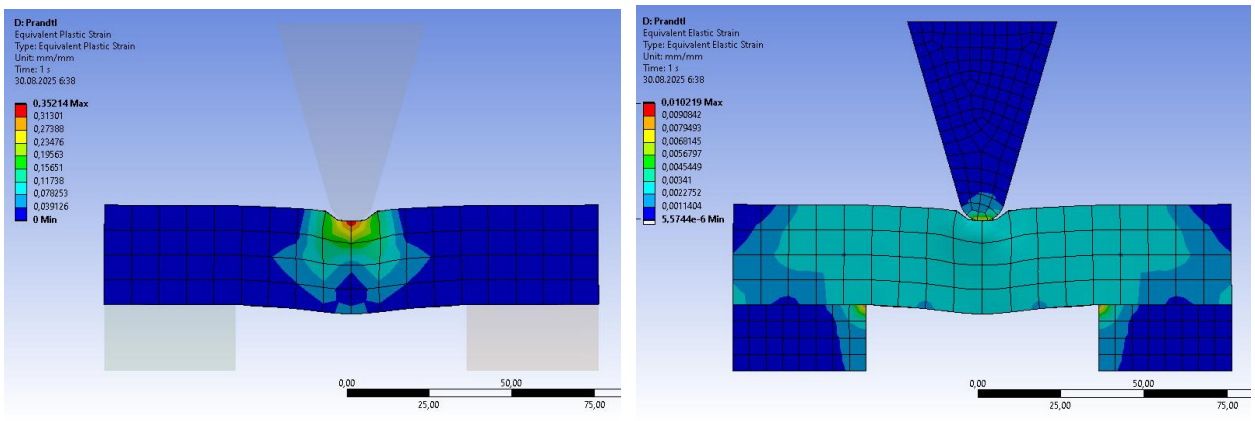

a b

Fig. 3. FEM model that reflects deformations in a granite sample for the Prandtl rheological model: a – plastic deformations; b – elastic deformations

The stress-strain graph using the Prandtl model is presented in Fig. 4. Analyzing the plastic Prandtl model, one can notice the absence of a curve that reflects the process of unloading the material, Fig. 4. The reason is that to display such a curve in Ansys, it is necessary to use appropriate nonlinear material models. In turn, the difference between the loading curve and the unloading curve symbolizes the energy expenditure for plastic deformation, the formation of defects, and the dissipation of energy in the form of heat.

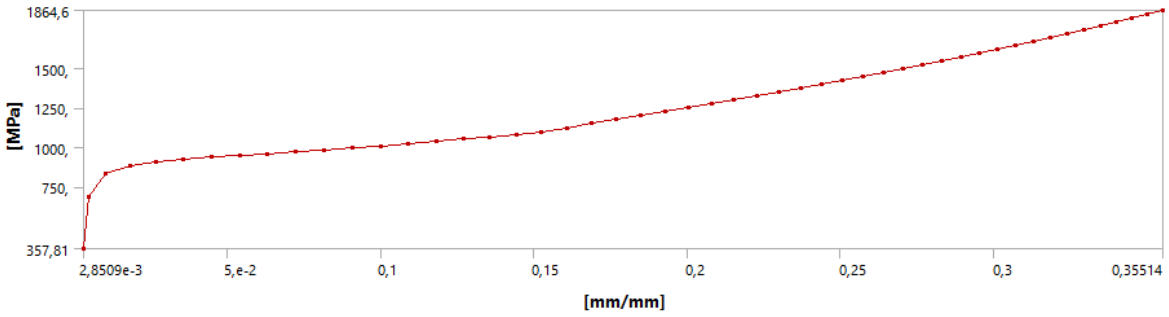

Fig. 4. Graph of the dependence of the change in stress on deformation for the Prandtl rheological model

Next, let's consider the Bingham model. Just like the Prandtl model, the pure Bingham viscoplastic model is not available in Ansys.

Common viscoplastic models available in Ansys are: 1) Anand model (modeling of high-temperature viscoplasticity); 2) Piercy model (modeling of cyclic viscoelastic hardening); 3) exponential viscous hardening model (viscoplastic hardening of materials); 4) Perzhin (general model of viscoplasticity taking into account strain rate).

Thus, to reproduce the Bingham model, it is possible to use an existing model with defined boundary conditions. The Perzhina model is best suited for these problems. To reproduce the Bingham model, it is necessary to take the parameter n (strain rate hardening exponent 1) equal to unity. The Perzhina model determines how the material develops plastic deformations and their speed, but does not give an answer where exactly the plastic deformations begin. Therefore, in this case, it is necessary to add a plastic model (bilinear isotropic hardening or multilinear isotropic hardening) to the Perzhina model.

Based on the above calculations, the Bingham viscoplastic model was calculated, the deformation and stress fields of which are presented in Fig. 5. The stress and deformation pattern was constructed for the case of applying a load of 50,000 N.

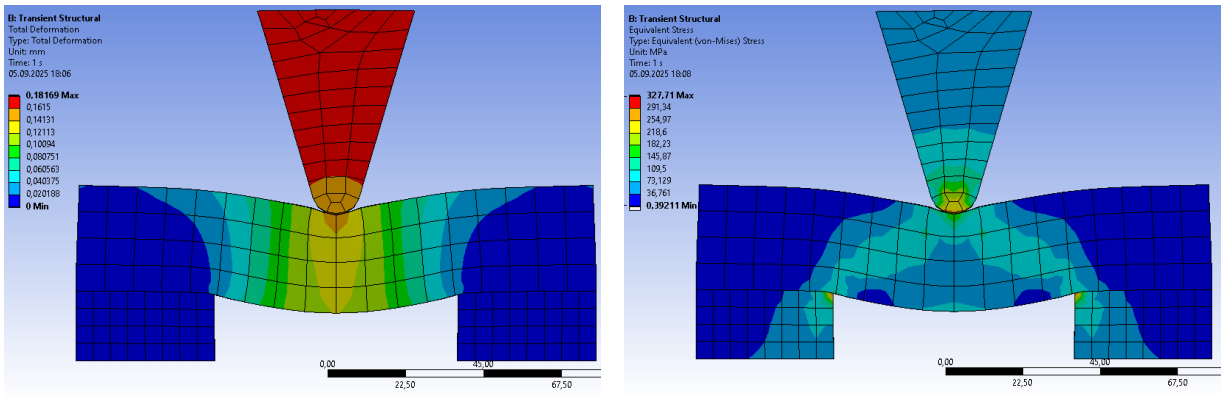

a b

Fig. 5. FEM model that reflects the picture of deformations and stresses in a granite sample for the Bingham rheological model: a – deformation field; b – stress field

The stress-strain graph for the Bingham model is presented in Fig. 6.

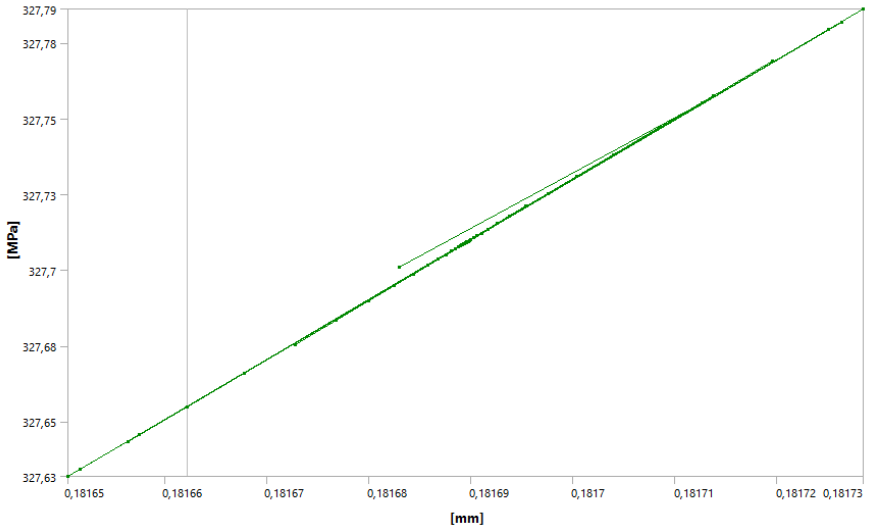

Fig. 6. Graph of the dependence of the change in stress on strain for the Bingham rheological model

It should be noted here that for a more accurate representation of the stress and strain pattern for the viscoplastic model, it is necessary to perform simulation in the transient structural module.

This is due to the fact that time dependencies are introduced in this model. It should be noted separately that in Ansys you can use the Explicit dynamic module, but its difference is that it is best suited for modeling processes with high loading rates, while transient structural is designed for modeling processes close to static.

The next step is to consider a more complex rheological model of Coulomb-Mohr. Due to the wide range of crushing machines, it is necessary to take into account, in addition to different material models, different shapes of the geometric surface of the crushing working bodies. To all this, it is necessary to add a complex loading condition in most crushing chambers of crushing machines. Let us summarize in Table 1 the physical characteristics of the studied geological rocks.

Table 1. Physical characteristics of rocks

Physical properties	Type of material			
	Marble	Granite	Gabbro	Gneiss
Initial angle of internal friction, radian	0,44156	0,89011	0,75	0,488
Initial cohesion, MPa	21,2	31.68	34,87	30.4
Dilatancy angle, radian	0,44156	0,89011	0,75	0,488
Residual angle of internal friction, radian	0.22078	0.445055	0.375	0.244
Residual cohesion, MPa	6,5	9,8	10.8	9.4
Source	[8],[9]	[8], [9],[10]	[8],[9],[10]	[8],[9]

In Table 1, the unknown parameters are: 1) the angle of internal friction; 2) cohesion. These parameters are necessary when solving the stress state problem based on the Coulomb-Mohr model. The angle of internal friction can be determined based on the following relationship:

$$\varphi = \left(\sin\left[\frac{6am_b\left(s + m_b\sigma_{3n}\right)^{a-1}}{2\left(1+a\right)\left(2+a\right) + 6am_b\left(s + m_b\sigma_{3n}\right)^{a-1}} \right] \right)^{-1}, \quad (1)$$

where a, m_b, s – Hoek-Brown criteria; $\sigma_{3n} = \sigma_{3max}/\sigma_в$ – coefficient; σ_{3max} – normal stress, which corresponds to the upper limit of agreement between the Coulomb-Mohr and Hoek-Brown theories; $\sigma_в$ - ultimate strength under uniaxial loading for the corresponding material.

Let us write down the definitions for the Hoek-Brown criteria. The criterion a is determined based on the following dependence:

$$a = \frac{1}{2} + \frac{1}{6}\left(e^{-GSI/15} - e^{-20/3}\right), \quad (2)$$

Criterion s:

$$s = e^{\left(\frac{GSI-100}{9-3D}\right)}, \quad (3)$$

Criterion m_b:

$$m_b = m_i e^{\left(\frac{GSI-100}{28-14D}\right)}, \quad (4)$$

where m_i – Hoeck-Brown constant (determined either based on laboratory tests or taken from a table [11]); GSI – geological index of rock strength (taken from the table [11]); D – a factor that depends on the degree of disruption of the crystal lattice during the extraction of rock from a rock massif and the relaxation of stresses. It is taken equal to 0 when considering rock in a mountain massif and 1 when considering rock extracted from a mountain massif.

Cohesion is a component of the strength under shear stresses. The cohesive strength is determined based on the following relationship:

$$c = \frac{\sigma_в \left[(1+2a)s + (1-a) m_b \sigma_{3n} \right] (s + m_b \sigma_{3n})^{a-1}}{(1-a)(2+a)\sqrt{1 + \left(6a m_b (s + m_b \sigma_{3n})^{a-1} \right) / \left((1+a)(2+a) \right)}} \quad , \tag{5}$$

Then the tangential stress according to the Coulomb-Mohr theory will be equal to [12], [13]:

$$\tau = c + \sigma \sin \varphi \tag{6}$$

The difficulty in determining cohesion and the angle of internal friction lies in determining the coefficient σ_{3n}. For this purpose, it is necessary to consider the main stresses acting on the material and their relationship under different theories. So, according to the Coulomb-Mohr theory, the normal principal stress on an arbitrary area of the material is determined as follows:

$$\sigma_1^{km} = \frac{2c \cos \varphi}{1 - \sin \varphi} + \frac{1 + \sin \varphi}{1 - \sin \varphi} \sigma_3^{km} \quad , \tag{7}$$

where σ_3^{km} – normal stress acting on the area perpendicular to the stress σ_1^{km}.

According to the Hoek-Brown theory, similarly to (7), the principal stress on an arbitrary area is determined by:

$$\sigma_1^{hb} = \sigma_3^{hb} + \sigma_в \left(m_b \frac{\sigma_3^{hb}}{\sigma_в} + s \right)^a \quad . \tag{8}$$

Next, to determine the stress σ3max, it is necessary to construct graphs for the principal stresses according to the corresponding equations (7) and (8), on the basis of which to determine the upper limit of their similarity.

Analyzing equations (7) and (8) it was found that for strong materials, such as granite, gabbro, gneiss, marble, the coefficient σ3n tends to zero. Based on this and the angle of internal friction φ taken from tabular values [8], [14], the cohesive strength for the corresponding materials was determined. For verification, known tabular values of cohesion for individual materials were used. The difference from the calculated values was less 5%.

To determine the dilatancy angle, the following relationship can be used:

$$\psi_д = \frac{\varphi}{1 + \log_{10} \sigma_в} \log_{10} \frac{\sigma_в}{\sigma_3 + 0.1} \quad , \tag{9}$$

Residual cohesion and friction angle are parameters that help describe the process of crack propagation in rock during deformation. This approach is used in the model CSFC (cohesive softening – constant friction), CSFH (cohesive softening – friction strengthening), CWFS (cohesive weakening – increased friction) [8],[15]. These models are designed for detailed investigation of crack growth and are based on the Coulomb-Mohr and Hoek-Brown criteria..

In [15] it is noted that the cohesion drop can be determined based on the following dependence:

$$c = c_i \exp\left[-\left(\frac{\varepsilon^p}{\varepsilon^p_{c,r}}\right)^2\right], \quad (10)$$

where ε^p – plastic deformation; c_i – initial cohesion; $\varepsilon_{c,r}^p$ – effective plastic deformation at which cohesion reaches its residual value.

In this case, the residual friction angle is proposed to be determined based on the following dependence:

$$\sin\varphi = \begin{cases} 2\dfrac{\sqrt{\varepsilon^p \varepsilon^p_{\varphi,r}}}{\varepsilon^p + \varepsilon^p_{\varphi,r}} \sin\varphi_r, & \varepsilon^p < \varepsilon^p_{\varphi,r} \\ \sin\varphi_r, & \varepsilon^p > \varepsilon^p_{\varphi,r} \end{cases}, \quad (11)$$

where $\varepsilon_{\varphi,r}^p$ – effective plastic deformation at which the friction angle reaches its residual value; φ_r – initial friction angle.

The use of dependencies (10) and (11) has difficulties in determining the effective plastic deformation. For the model CWFS it is assumed that cohesion reaches its residual value at $\varepsilon_{c,r}^p$ = 0,2%, while the residual friction angle reaches its maximum value at $\varepsilon_{\varphi,r}^p$ = 0,5%.

For the model CSFC in [15], another dependence was proposed for determining residual cohesion:

$$c = c_i\left(1 - \frac{\tanh(100\gamma_p)}{\tanh(10)} + 0.001\right)^n, \quad (12)$$

where γ_p – shear plastic deformation; h – parameter; n – a parameter that determines the type of material (related to the texture of the material and the size of the grains that make up the material). Determined experimentally [15].

The parameter h can be determined based on the following relationship:

$$h = -\sqrt{\left[1/3\left(1+\sin(\varphi)\sin(\psi)\right)\right]}\frac{d\sigma_1^{km}}{d\eta}, \quad (13)$$

where ψ – dilatancy angle; η – parameter that is a function of the input material parameters, after passing peak loads. In this case η is a function of a set of parameters that determine the residual cohesion of the material.

The plasticity coefficient in dependence (12) is equal to γ_p = 0 when cohesion reaches its maximum value, i.e. at peak strength. With residual cohesion γ_p = 10%.

In [11], [12] for the model CWFS it is proposed to determine the residual cohesion and the friction angle based on the dependencies:

$$c = c_r + (c_i - c_r)\left[2 - \frac{2}{1+\exp(-5\frac{\varepsilon^p}{\varepsilon^p_r})}\right], \quad \varphi = \varphi_i + (\varphi_r - \varphi_i)\left[\frac{2}{1+\exp\left(-5\frac{\varepsilon^p}{\varepsilon^p_r}\right)} - 1\right], \quad (15)$$

where c_r – residual cohesion (in [11], [12] the values are taken $c_r = 0{,}3c_i$ for limestone); φ_r - friction angle at residual cohesion.

In the models considered above, the dependences (10) - (15), the meaning of plastic deformation is not clear. So for materials that behave plastically, the determination of plastic deformation will not have significant difficulties. However, for elastic-plastic or elastic-visco-plastic models, the

determination of the proportion of plastic deformation will be difficult. Therefore, such models require experimental refinement.

If we consider crushing machines and the processes that occur in them more broadly, then for dynamic fracture, this model for describing the process of crack propagation, namely the loss of material strength, will not be accurate.

Let us plot graphs of the dependence of plastic shear deformations on cohesive strength (Fig. 7) for the materials presented in Table 1.

The value of plastic deformation was taken within 1 mm. Based on which the residual cohesion for the corresponding materials was determined. All data on residual cohesion are listed in Table 1. For each material, three cases were considered, namely when the effective deformation is ε_{cp} = 0.2%, 0.5%, 1%. In general, as noted in [14] and [15], the value of residual cohesion at different percentages of plastic deformation is the same and starts from 0,2%.

To determine the residual friction angle according to formula (16), it is necessary to determine the friction angle at residual cohesion φ_r.

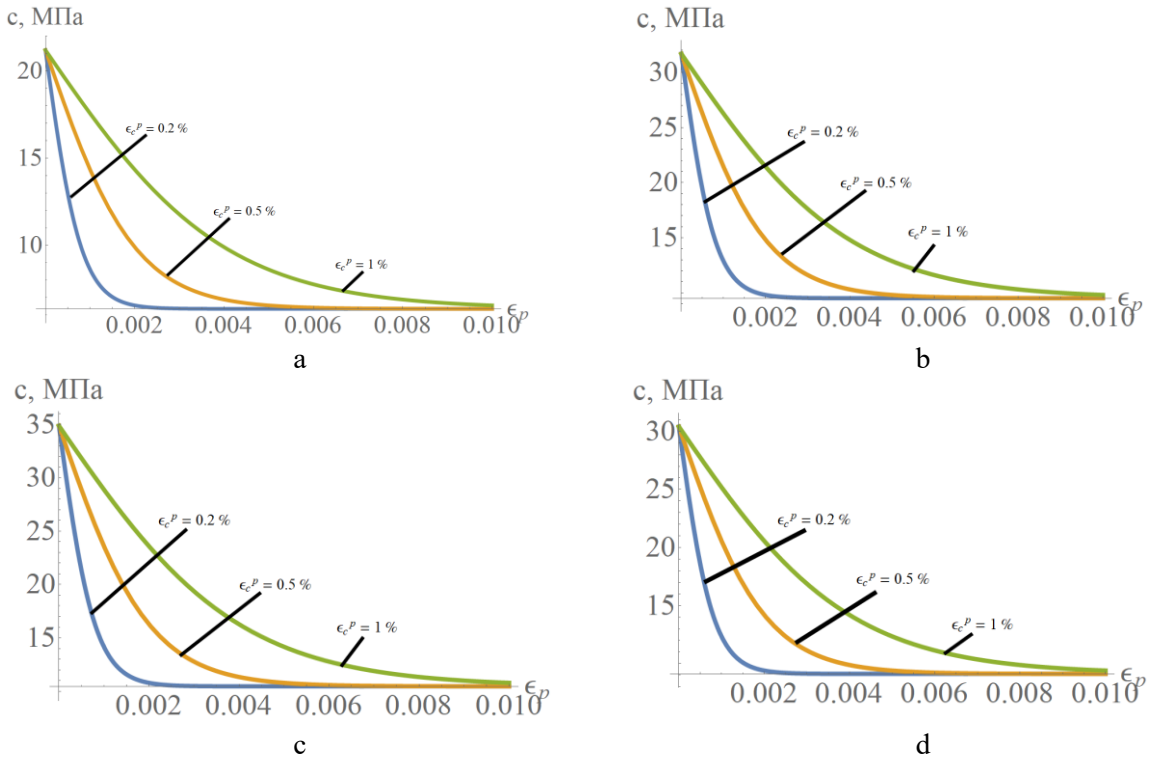

Fig. 7. Residual cohesion depending on plastic shear deformation:
a – marble; b – granite; c – gabbro; d- gneiss

Based on the calculated parameters of the material models, we create a corresponding library in Ansys and perform the corresponding calculations. To reproduce the crushing chamber of the jaw crusher, two models were prepared, which include two plates that compress the material in the form of a sphere. The size of the sphere – D = 100 mm, Fig. 8.

As we can see, the stress pattern for the tested rocks is similar, Fig. 8. The graph of normal stresses in the direction of the X and Z axes for the granite material is presented in Fig. 9, a.

The results of the stress pattern are consistent with those presented in [11], [18]. The highest stresses at the beginning of compression occur at the points of contact of the material and the crushing plate. In the center of the rock, the stresses are much lower. With a further increase in the load, the point of contact of the material and the plate increases, due to possible chipping, elastic deformation, compaction of the contact zone, etc.

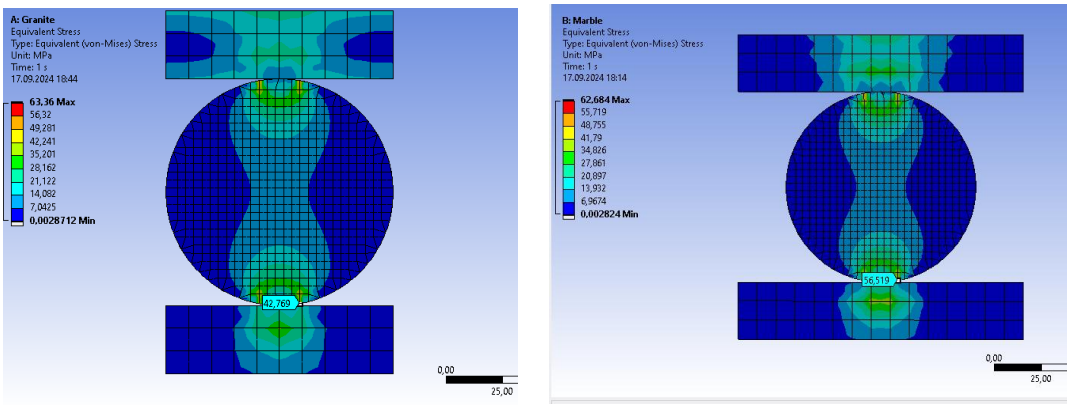

a b

Fig. 8. Stress pattern of rocks under compressive loading:
a – granite; b – marble.

As a result, the stress concentration on the contact surface decreases, which can lead to the onset of fractures in the central part of the sample.In [18], significant differences in the stress patterns of homogeneous and heterogeneous materials in terms of structure are noted. If we take into account the fact that most building rocks are heterogeneous materials, i.e. heterogeneous, it follows that it is better to use a discrete approach for modeling such materials, because the heterogeneity of the rock can have a local effect on the stress fields.

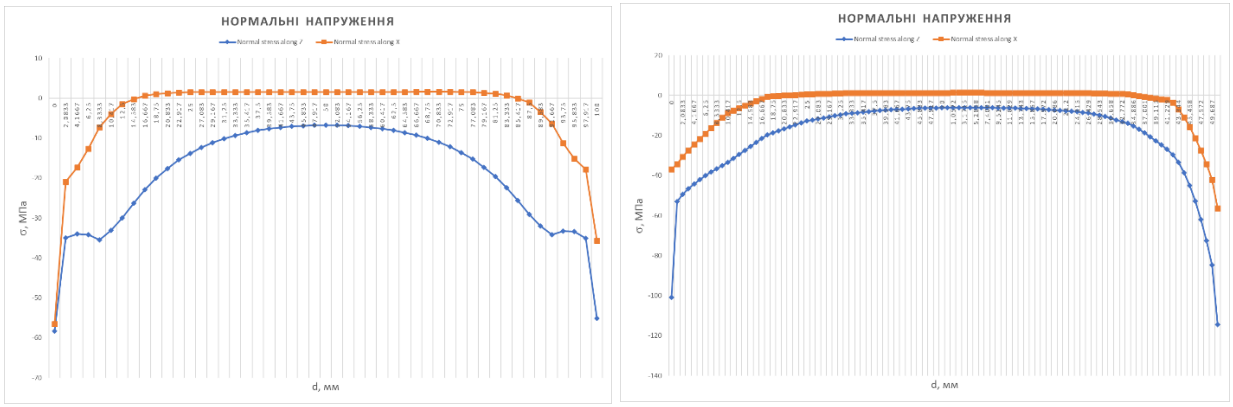

a b

Fig. 9. Normal stresses along the X and Z axes when loaded:
a - by flat working bodies; b - by wedge working bodies

In [17], [19] it is noted that if flat steel plates are used to load the sample, then the contact width and contact stresses can be determined based on the following equation:

$$\frac{b}{D} = 2\left(\frac{2F}{\pi Dt}\right)^{1/2}\left[\frac{1-\nu_p^2}{E_p}+\frac{1-\nu_s^2}{E_s}\right]^{1/2}, \qquad (16)$$

where b – contact patch width; D – material diameter; F – load; t – material thickness; ν_p and ν_s - Poisson's ratio of the plate and the material, respectively; E_p and E_s – modulus of elasticity of the plate and material. Fig. 10 shows the picture of stresses in the material due to the application of load to it by wedge-shaped working bodies.

Comparing the stress patterns when loads are applied by flat working bodies and wedge-shaped ones, it becomes clear that the stresses in the material are an order of magnitude higher when using wedge-shaped working bodies. And here it can be noted that the smaller the width of the wedge pad at the contact point, the higher the stress concentration will be. To select the required pad, you can use equation (16).

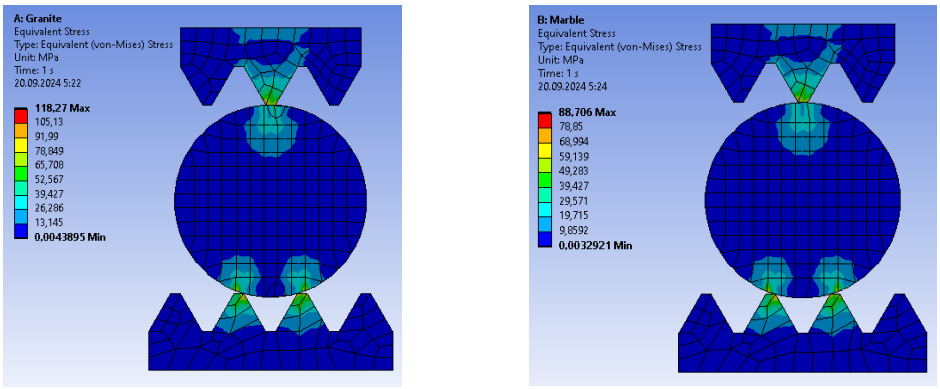

a b

Fig. 10. Stress pattern under conditions of applying load by wedge-shaped working bodies: a – granite; b – marble

The normal stress plot along the Z and X axes is shown in Fig. 9b, which shows significantly higher stresses in the contact zones and has a flatter section closer to the center of the material. This also indicates the mechanism of crack formation and the onset of material failure in the contact zone.

6. Discussion. Based on the considered rheological models in the Ansys software complex, it was established that to study the fracture of materials that have elastic-plastic or plastic properties, it is necessary to use such rheological models as Bilinear Isotropic Hardening or Multilinear Isotropic Hardening. When adopting appropriate boundary conditions for these models, we will obtain Saint-Venant or Prandtl rheological models. When considering energy costs in the process of material fracture, it is important to understand the amount of energy required for the formation and propagation of a crack. During the fracture process, some of the energy is spent on accompanying processes or dissipated in the form of heat. In elastic-plastic, plastic and viscoplastic materials, some of the energy is dissipated on deformation that does not lead to the fracture of the sample. That is, this may be chipping of protruding edges of the material, redistribution of grains of the internal structure, nucleation of a crack system. On the load diagram, such processes are displayed by an unloading curve that does not coincide with the initial load curve. From the studies considered above, it can be noted that the rheological models Bilinear Isotropic Hardening or Multilinear Isotropic Hardening do not reflect the processes of energy dissipation, which is a direction of further research. When considering the rheological model of Pergin with the corresponding boundary conditions in the graph of Fig. 6, the mismatch of the loading and unloading curves is noticeable. The study of the use of the Coulomb-Mohr model indicates a significant number of experimental parameters that must be taken into account. Important parameters of the material destruction process are the internal friction angle and the cohesive strength of the material. For a complete description of the destruction pattern, which will correspond to most crushing machines and the establishment of relevant patterns, it is necessary to further consider the features of the dynamic loading of materials. Additionally, under the condition of considering static loading, it is necessary to consider another common rheological model Drucker-Prager, which is generally better suited for analysis by the finite element method.

7. Conclusions The paper defines the corresponding patterns of fracture of materials with different physical and mechanical properties and under different geometry of crushing plates. The patterns of stresses and deformations of materials with different physical and mechanical properties are considered, under the conditions of using different rheological models. Under conditions of static loading in elastic-plastic, plastic and viscoplastic rheological models of rocks, part of the energy is spent on deformation, which does not lead to the destruction of the rock. The parameters of the Coulomb-Mohr rheological model are determined, graphs of the dependence of cohesion on plastic shear deformation are constructed taking into account the effective plastic deformation. It is established that wedge-shaped working elements of crushing machines create greater stresses compared to flat ones. An analysis of the dependence that determines the rational width of the contact

surface of the working elements of crushing machines depending on the load and physical and mechanical properties of the contacting bodies is performed.

References:

1. Ye. O. Mishchuk, I.I. Nazarenko (2023) Analysis of the energy laws of material destruction. Strength of Materials and Theory of Structures. 2023. № 110, p. 294-315. https://doi.org/10.32347/2410-2547.2023.110.294-315.
2. Evertsson, C. M., & Bearman, R. A. (1997) Investigation of interparticle breakage as applied to cone crushing. Minerals Engineering, 10(2), 199–214. https://doi.org/10.1016/S0892-6875(96)00146-X.
3. Nikolov, S. (2002) Modelling and simulation of particle breakage in impact crushers. Minerals Engineering, 15(10), 715–720. https://doi.org/10.1016/S0892-6875(02)00074-6.
4. Irani, N., Tafili, M., Salimi, M., Goudarzy, M., & Wichtmann, T. (2025) Particle breakage: Exploring the numerical and experimental approaches in crushable soil mechanics. Archive of Applied Mechanics, 95, Article 151. https://doi.org/10.1007/s00419-025-02845-0.
5. Tang, C. A., Xu, X. H., Kou, S. Q., Lindqvist, P.-A., & Liu, H. Y. (2001). Numerical investigation of particle breakage as applied to mechanical crushing—Part I: Single-particle breakage. Powder Technology, 122(2–3), 109–120. https://doi.org/10.1016/S1365-1609(01)00075-2.
6. Cleary, P. W., & Sinnott, M. D. (2015). Simulation of particle flows and breakage in crushers using DEM: Part 1 – Compression crushers. Minerals Engineering, 74, 178–197. https://doi.org/10.1016/j.mineng.2014.10.021.
7. Briggs, C. A., & Bearman, R. A. (1996). An investigation of rock breakage and damage in comminution equipment. Minerals Engineering, 9(5), 489–497. https://doi.org/10.1016/0892-6875(96)00037-4.
8. ANSYS. (2025). ANSYS Mechanical APDL material reference (v25.1) [Manual]. ANSYS, Inc. https://ansyshelp.ansys.com/public/account/secured?returnurl=/Views/Secured/corp/v251/en/ans_mat/ans_mat.html.
9. Sinha, R.S., Mukhopadhyay, A.K. Failure analysis of jaw crusher and its components using ANOVA. J Braz. Soc. Mech. Sci. Eng. 38, 665–678 (2016). https://doi.org/10.1007/s40430-015-0393-6.
10. C. Okechukwu1, O. A. Dahunsi, P. K. Oke, I. O. Oladele, M. Dauda and B. M. Olaleye Design and operations challenges of a single toggle jaw crusher: a review. Nigerian Journal of Technology (NIJOTECH) Vol. 36, No. 3, July 2017, pp. 814 – 821. http://dx.doi.org/10.4314/njt.v36i3.22.
11. Robert C. Dunne (2019) Mineral Processing & Extractive Metallurgy Handbook. Society for Mining, Metallurgy & Exploration, USA, p. 2258. ISBN 978-0-87335-385-4.
12. Gupta, A., & Yan, D. (2016). Mineral processing: Design and operations (2nd ed.). Elsevier.
13. Haldar, S. K. (2018). Mineral exploration: Principles and applications (2nd ed.). Elsevier.
14. Taggart, A. F. (1998). Hand book of ore dressing (pp. 255–280). John Wiley & Sons, Inc.
15. Bearman, R.T. Jaw and Impact Crushers. In SME Mineral Processing and Extractive Metallurgy Handbook; Society for Mining, Metallurgy, and Exploration, Inc.: Englewood, CO, USA, 2019; p. 367.
16. Murithi, M., Keraita, J.N., Obiko, J.O. et al. Optimisation of the swinging jaw design for a single toggle jaw crusher using finite element analysis. Int J Interact Des Manuf 18, 6351–6358 (2024). https://doi.org/10.1007/s12008-022-01044-3.
17. Wang Yalei, Lv Kun, Chen Zongyuan The Optimization of Jaw Crusher with Complex Motion Aimed at Reducing Stroke Feature Value of Its Outlet. International Journal of Engineering and Technical Research (IJETR) ISSN: 2321-0869 (O) 2454-4698 (P) Volume-8, Issue-01, January 2018.
18. Donovan, J. G. (2003). Fracture toughness based models for the prediction of power consumption, product size, and capacity of jaw crushers (Doctoral dissertation, Virginia Polytechnic Institute and State University). Virginia Tech Electronic Theses and Dissertations.
19. Ciężkowski, P., Maciejewski, J., Bąk, S., & Kwaśniewski, A. (2020). Application of the new shape crushing plate in machine crushing processes. Studia Geotechnica et Mechanica, 42(1), 83–96. https://doi.org/10.2478/sgem-2019-0029.